Journal of Hydrology 496 (2013) 154–165

Contents lists available at SciVerse ScienceDirect

Journal of Hydrology

journal homepage: www.elsevier.com/locate/jhydrol

Modeling earthen dikes using real-time sensor data

N.B. Melnikova *, V.V. Krzhizhanovskaya, P.M.A. Sloot *

University of Amsterdam, Science Park 904, 1098 XH Amsterdam, The Netherlands
National Research University ITMO, Birzhevaya line 4, Saint-Petersburg 199034, Russia

ARTICLE INFO

Article history:
Received 5 February 2013
Received in revised form 4 May 2013
Accepted 7 May 2013
Available online 24 May 2013
This manuscript was handled by Corrado Corradini, Editor-in-Chief, with the assistance of Gokmen Tayfur, Associate Editor

Keywords:
Dike stability
Porous flow
Diffusivity calibration
Sensitivity analysis
Live sensor data

SUMMARY

The paper describes the concept and implementation details of integrating a finite element module for dike stability analysis "*Virtual Dike*" into an early warning system for flood protection. The module operates in real-time mode and includes fluid and structural sub-models for simulation of porous flow through the dike and for dike stability analysis. Real-time measurements obtained from pore pressure sensors are fed into the simulation module, to be compared with simulated pore pressure dynamics. Implementation of the module has been performed for a real-world test case, an earthen levee protecting a sea-port in Groningen, The Netherlands. Sensitivity analysis and calibration of diffusivities have been performed based on pore pressure sensor data during tidal fluctuations. An algorithm for automatic diffusivities calibration for a heterogeneous dike is proposed and studied. Analytical solutions describing tidal propagation in a one-dimensional saturated aquifer are employed in the algorithm to generate initial estimates of diffusivities.

1. Introduction

Regular floods pose a serious threat to human life, valuable property and city infrastructure. Many international projects are aimed at the development of flood protection systems (Krzhizhanovskaya et al., 2011; Pengel et al., 2013). The European Union Framework Programme 7 (FP7) project *SSG4Env* is focused on development of semantic sensor grids for environmental protection. The *Flood Probe* FP7 project coordinates related work on combining sensor measurement techniques. A big national Dutch project *Flood Control 2015* aims to share sensor measurements datasets and to provide a user interface to explore sensor data for researchers, technical maintainers and civil population. The *IJkDijk* (http://www.ijkdijk.nl) is a project on experimental physical study of dike failure mechanisms. The tests are carried out on full-scale experimental dikes equipped with large sets of sensors. The project has produced extremely detailed datasets of sensor data, including pore pressures, inclinations, stresses and strains. Our research was conducted under the *UrbanFlood* FP7 project (http://www.urbanflood.eu), which unites the work on monitoring dikes with sensor techniques (Pyayt et al., 2011a), physical study of dike failure mechanisms (Krzhizhanovskaya et al., 2011), and software development for dike stability analysis (Melnikova et al., 2011a; Pyayt et al., 2011b), simulation of dike breaching, flood, and city evacuation (Melnikova et al., 2011b; Gouldby et al., 2010; Mordvintsev et al., 2012).

The early warning system is a multi-component system that runs in real-time mode, gathering and analyzing measurements form sensors installed in dikes, predicting dike stability, possibility of flooding and optimal evacuation routes. A general workflow and interaction of software components in the *UrbanFlood* early warning system are presented in Fig. 1.

The *Sensor Monitoring* module receives data streams from the sensors installed in the dike. Raw sensor data are filtered by the *AI* (*Artificial Intelligence*) *Anomaly Detector* that identifies abnormalities in dike behavior or sensor malfunctions. The *Reliability Analysis* module calculates the probability of dike failure in case of abnormally high water levels or an upcoming storm and extreme rainfalls. If the failure probability is high then the *Breach Simulator* predicts the dynamics of a possible dike failure, calculates water discharge through the breach and estimates the total time of the flood. After that, the *Flood Simulator* models the inundation process and *Evacuation Simulator* optimizes evacuation routes. Then *Risk Assessment* module calculates flood damage. Finally, *Decision Support System* provides access to different information levels, for experts and citizens. The simulation modules and visualization components are integrated into the Common Information Space

* Corresponding authors at: National Research University ITMO, Birzhevaya line 4, Saint-Petersburg 199034, Russia. Tel.: +7 921 319 65 31.
E-mail address: N.Melnikova@uva.nl (N.B. Melnikova).

0022-1694
http://dx.doi.org/10.1016/j.jhydrol.2013.05.031

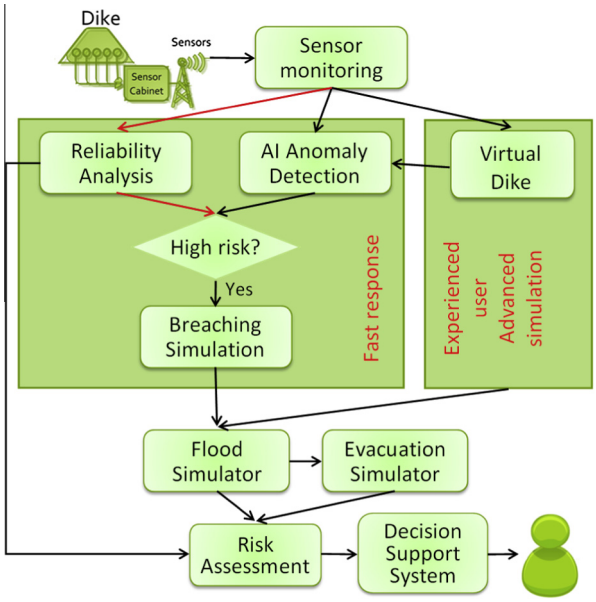

Fig. 1. Early warning system workflow.

(Balis et al., 2011). They are accessed from the interactive graphical environment of a multi-touch table or through a web-based application.

The *Virtual Dike* component runs in parallel with the *Reliability Analysis* module, offering direct numerical simulation to analyze dike stability under specified loadings (Melnikova et al., 2011a). The module can be run with a real-time input from water level sensors or with predicted high water levels due to upcoming storm surge or river flood. In the first case, comparison of simulated pore pressures with real data can indicate a change in soil properties or in dike operational conditions (e.g. failure of a drainage facility). In the second case, simulation can predict the structural stability of the dike and indicate the "weak" spots in the dikes that require attention of dike managers and city authorities. Simulated dynamics of dike parameters (including local and overall stability, pore pressure, local stresses and displacements) describes the non-stationary behavior of the dike (changing over time) We define a concept of a "virtual sensor" for the data obtained from finite element solution in the point where a real sensor is located. Data from the virtual sensors are compared to the real-life sensor measurements. The result of the *Virtual Dike* simulations are used to train the Artificial Intelligence system on "normal" and "abnormal" virtual sensor dynamics (Pyayt et al., 2011b).

The EWS is described in detail in (Balis et al., 2011). In the current paper we only focus on the *Virtual Dike* module design.

Dike stability analyses under hydraulic and structural loads are usually carried either by probabilistic breach analyses based on empirical engineering criteria (Vorogushyn et al., 2012) or by direct simulation techniques including conventional limit equilibrium methods (Verruijt, 2001) and finite element modeling of dike deformations (for example, Spencer and Hicks, 2007). While the first approach is more robust and is widely used for dike stability analysis, the second approach, especially finite element analysis, allows more profound study of physical processes occurring in the dike before the actual failure. Under the frame of the *UrbanFlood* project we create a number of pre-defined and calibrated structural stability analysis models for the dikes connected to the early warning system. Realistic modeling of water flow through the dikes is necessary for correct estimation of effective stresses in the dikes and hence for predicting their stability. Calibration of diffusivities for the tidal groundwater flow is often performed by tidal methods (Smith and Hick, 2001; Slooten et al., 2010; Williams et al., 1970) based on one-dimensional analytical models of semi-infinite or finite aquifers. This method is suitable for aquifers with nearly horizontal phreatic surfaces. A more accurate way that works well for high amplitude of water level variation is direct numerical simulation. In the present work, both analytical and numerical approaches have been tested and compared. Calibration of diffusivities of soil strata has been performed by matching tidal pore pressure fluctuations obtained from numerical simulation and from piezometers installed in several cross-sections of the dike. For heterogeneous soil structures, some averaged and simplified yet heterogeneous soil build-ups have been obtained, so that the response of the dike to the tidal load corresponds well to sensor measurements.

Tidal oscillations of sea level influence the position of a phreatic surface in the dike. A moving water table creates zones with partially saturated soil. Resistance of porous media to the flow is modeled by Darcy's law suitable for low flow velocities (Bear, 1979). A problem of unconfined porous flow can be solved either by solving Darcy's equation on a moving mesh with adjusting mesh boundary to coincide with surface of zero pore pressure (Fenton and Griffiths, 1997), or by using a stationary mesh and solving Richards' equation with non-linear rheological properties for the media, dependent on the effective water content. These non-linear properties can be modeled by classical models of Van Genuchten (1980) or Brookes and Corey model (Brooks and Corey, 1966), as well as by other approximations of water retention curves (Bathe and Khoshgoftaar, 1979) simplified for faster numerical convergence. We have used Richards' equation with the Van Genuchten model, performing simulations on a fixed mesh.

In this paper we present numerical and analytical results of sensitivity analysis of the porous flow parameters to the variation of soil diffusivity and calibration results performed for the LiveDike, an earthen sea dike in Groningen, The Netherlands. Some preliminary results have been published in (Krzhizhanovskaya and Melnikova, 2012). Now we present a more extensive study of the problem, complementing numerical simulations by analytical analysis, and suggesting an algorithm for *automatic* calibration of diffusivities for a heterogeneous dike.

2. LiveDike: geometry, soil build-up, loadings and sensor data

LiveDike is one of the research sites of the UrbanFlood project. It is an earthen sea dike protecting a seaport in Groningen, The Netherlands (Fig. 2a and b). The height of the dike is 9 m, the width is about 60 m and the length is about 800 m. The dike has a highly permeable sand core covered by a 60 cm thick clay layer.

The LiveDike has been equipped with sensors with GPS locations shown in Fig. 3a. Sensors are placed in four cross-sections (slices), see Fig. 3a and b. These slices have been simulated in 2D models under tidal water loading, in order to calibrate diffusivities, simulate flow through the dike and finally analyze the structural stability of the dike.

A geometric model of a dike slice with sensor locations is presented in Fig. 3c. Sensors E1–E4 and G1 and G2 measure absolute pore pressure and temperature and produce data stream which is available in real-time via a LiveDike Dashboard (http://livedijk-www.ict.tno.nl/). For calibration of the model, we used signals from the E3, E4 and G2 pore pressure sensors located below the phreatic surface. An input signal for simulation was the water level registered by the sensor installed outside of the dike (see Fig. 3c). The sea-side toe of the dike is located at $x = 0$ m, $y = -0.7$ m, while the mean sea level is at $y = 0$ m.

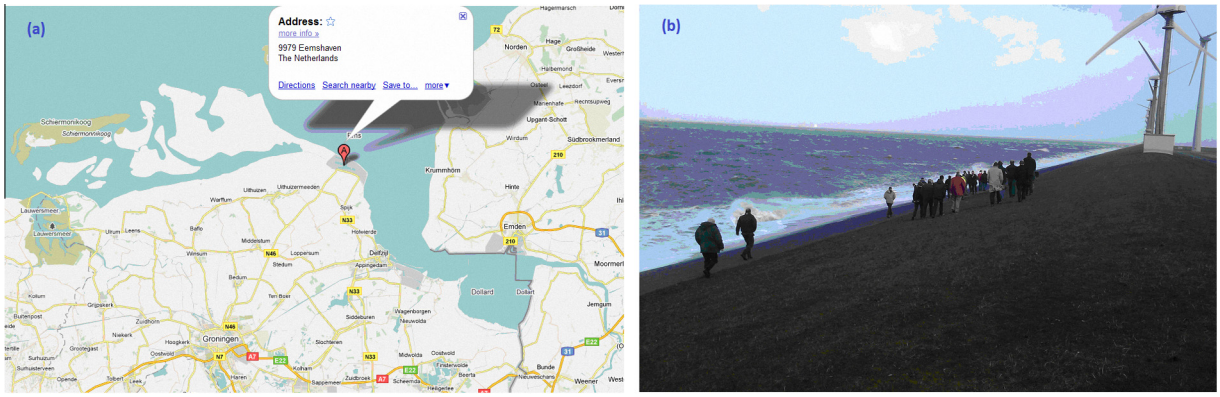

Fig. 2. LiveDike: (a) location of the test site near Groningen, The Netherlands and (b) photo of the dike.

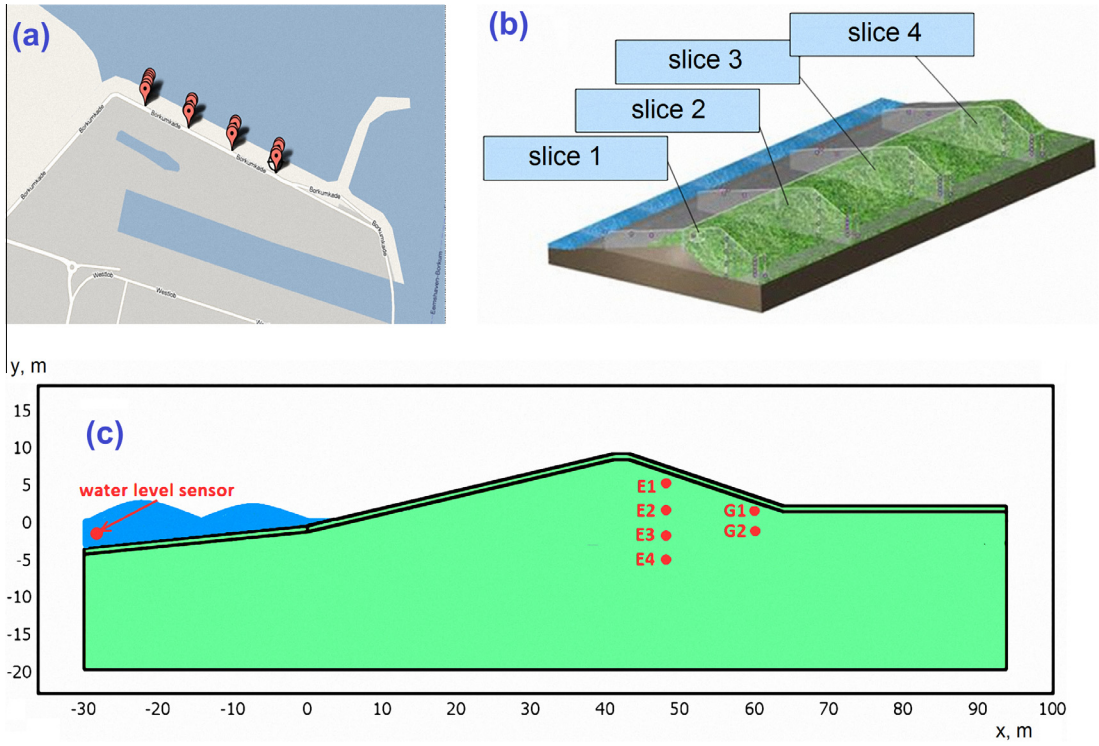

Fig. 3. (a) Top view at the LiveDike (Eemshaven). (b) Slices of the LiveDike. (c) 2D model of a dike slice with pore pressure sensor locations shown with red dots. (For interpretation of the references to color in this figure legend, the reader is referred to the web version of this article.)

The soil build-up for a longitudinal cross-section passing through the crest of the dike is presented in Fig. 4. It contains horizontal layers of sand (1-light orange[1]), silty sand with small clay inclusions (5-lemon) and 60 cm clay layer that covers the dike (2-blue). Gray areas (4) are clayey sand. Below the sand layers lies impermeable clay layer (3-blue). Cone penetration test (CPT) results (cone end resistance and frictional resistance) are schematically shown with black lines. More information on the CPT testing methodology can be found in (Meigh, 1987).

A sample of sensor data showing air pressure, sea level and pore pressure is presented in Fig. 5 and 6, for a time period that has been used for diffusivity calibration ("training period"). Sea level dynamics is presented in Fig. 5b, with positions of local maximum and minimum marked with dashed lines. Fig. 6 presents pore pressure measured in three slices of the dike. For calibration of diffusivities, the original pore pressure signals are smoothed (denoised) by a localized linear fit algorithm with an adaptive window (the smoothed signals are also shown in Fig. 6). Then the levels of minimal and maximal tidal pressure are detected for the smoothed pressure signals. These levels are shown in Fig. 6 with horizontal dashed lines. Corresponding pressure values are specified in the legends. Vertical dashed lines show the moments of time corresponding to the minimal and maximal pressure values. The corresponding time values are specified in the legends. The obtained relative pressure amplitudes and time delays between local pressure maximum and sea level maximum are presented in Table 1.

E3 and E4 sensors are located at the same distance from the sea ($x = 50$ m), but at the different levels ($y = -1.5$ m and $y = -5.5$ m from the reference level, correspondingly). E3 pressure oscillations are lower than E4 oscillations and this fact points to the presence of a vertical heterogeneity in the dike. A time delay between E4

[1] For interpretation of color in Fig. 4, the reader is referred to the web version of this article.

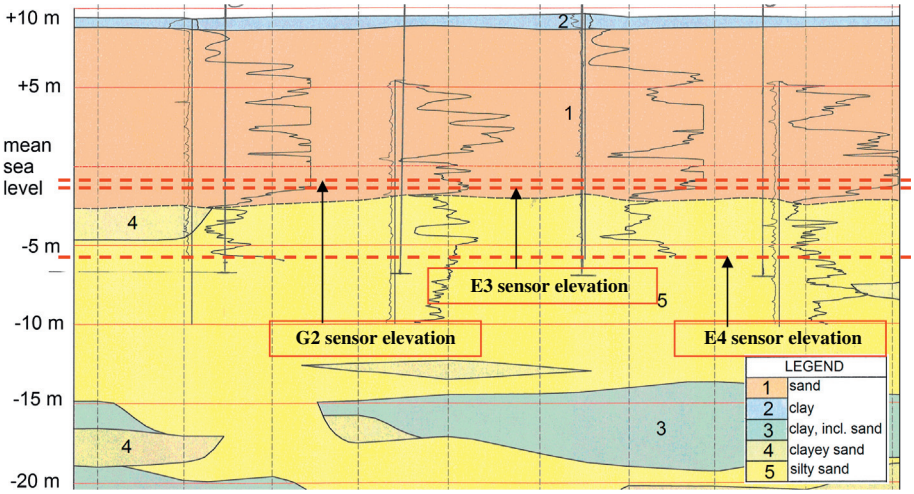

Fig. 4. Soil build-up in the LiveDike and underlying soil strata.

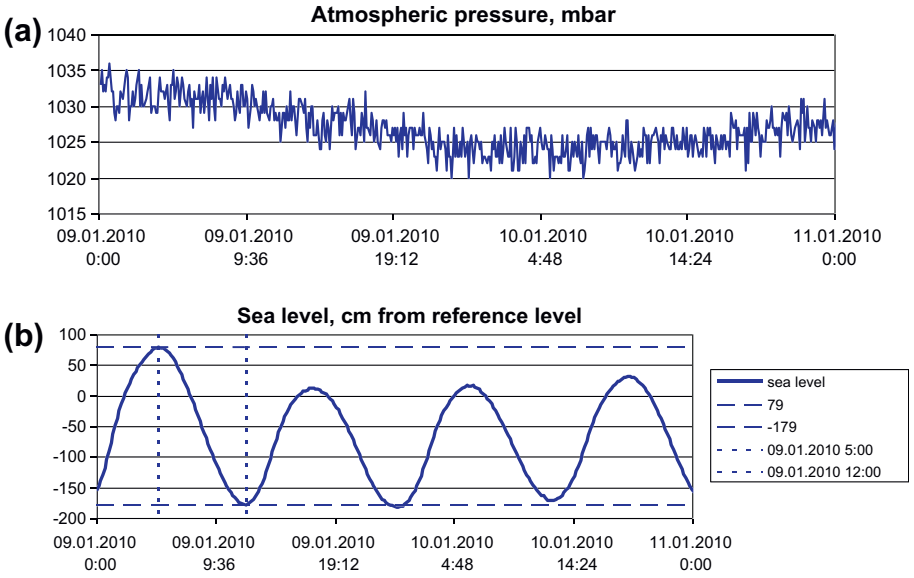

Fig. 5. LiveDike: (a) atmospheric pressure (mbar) and (b) sea level (cm) registered by sensors.

oscillations (at $x = 50$ m) and tidal oscillations (at $x = 0$ m) varies in the range between 3 and 18 min, which indicates highly permeable sand in the zone $0 < x < 50$ m. E3 oscillations lag from tidal oscillations by 9–38 min.

E3 and G2 sensors are located at approximately the same level (−1.2 m to −1.5 m from ref. level), but at different distances from the sea ($x = 50$ and $x = 62$ m, correspondingly). In the first slice, the amplitude of pore pressure dissipates quickly within 12 m of horizontal distance between E3 and G2 sensors (Table 1). It indicates the presence of a horizontal heterogeneity in the sand layers, with diffusivity decreasing with the distance from the sea, up to a dense impermeable zone near G2. This impermeable zone creates high time lag between G2 oscillations and tidal oscillations: the lag equals to 49 min in the first slice.

We have built a heterogeneous 2D model of the 1st slice of the LiveDike, in order to reproduce actual pore pressure fluctuations. In the following sections we present the mathematical model of porous flow, numerical and analytical studies of diffusivity influence on the pore pressure dynamics in the dike and calibration of diffusivities based on sensor data.

3. Mathematical model

Water flow through the dike is described by Richards' equation with the Van Genuchten model for water retention in partially saturated soil around the phreatic surface:

$$(C + \theta_e S)\frac{\partial p}{\partial t} + \nabla \cdot \left[-\frac{K_S}{\mu} k_r \nabla(p + \rho g z)\right] = 0, \quad (1)$$

where C, θ_e, S denote specific moisture capacity (1/Pa), effective water content and specific storage (1/Pa), respectively; $S = 1/K$, where K is soil skeleton bulk modulus; p is water pressure (negative in unsaturated zone), (Pa); t is time (s); $\nabla = \underline{e}_x \frac{\partial}{\partial x} + \underline{e}_y \frac{\partial}{\partial y} + \underline{e}_z \frac{\partial}{\partial z}$ is the Hamiltonian; K_S is permeability of saturated media (m^2); $k_r = k_r(p)$ is relative permeability; μ is dynamic viscosity of water (Pa s), (μ is a function of water temperature and changes its value during the year); g, ρ, z are standard gravity (m/s^2), water density (kg/m^3) and vertical elevation coordinate (m), respectively. Specific moisture capacity C and relative permeability k_r are described by Van Genuchten equations (Van Genuchten, 1980):

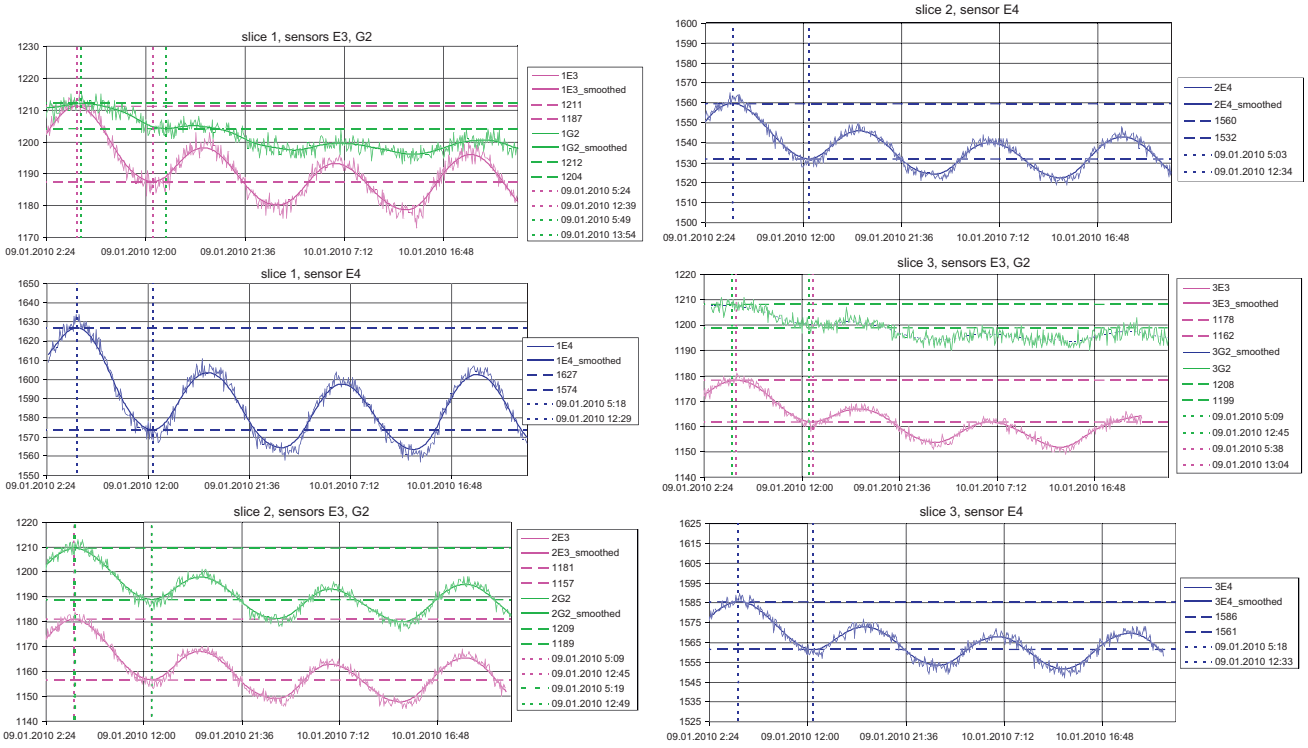

Fig. 6. LiveDike: absolute pore pressure (mbar) registered by sensors and smoothed (denoised) pressure signals in three dike slices.

$$C = \frac{\partial\theta}{\partial p} = \begin{cases} \frac{am}{1-m}(\theta_s - \theta_r)\theta_e^{1/m}\left(1-\theta_e^{1/m}\right)^m, & p < 0, \\ 0, & p \geqslant 0 \end{cases}, \quad (2)$$

$$k_r = \begin{cases} \theta_e^l\left[1-\left(1-\theta_e^{1/m}\right)^m\right]^2, & p < 0 \\ 1, & p \geqslant 0 \end{cases},$$

where θ is water content; θ_s and θ_r are saturated and residual water content, specific for each soil.

Effective water content is calculated as

$$\theta_e = \begin{cases} \frac{1}{(1+(a|p/\rho g|)^n)^m}, & p < 0 \\ 1, & p \geqslant 0 \end{cases}, \quad (3)$$

where a, n, $m = 1 - 1/n$, l are Van Genuchten parameters specific for each soil type (see Table 2 for these parameters values).

For the LiveDike, a planar slice of the dike has been modeled, with the boundary conditions specified as follows (Fig. 7): magenta boundaries are walls with zero normal flux $\frac{\partial p}{\partial n} = 0$; black boundaries are sea side with tidal pressure oscillations specified:

$$\begin{cases} p = \rho g \cdot (h(t) - y) & \text{for } y \leqslant h(t) \\ p = 0 & \text{for } y > h(t) \end{cases}, \quad (4)$$

where $h(t)$ is oscillating sea level (m), measured by sensors or predicted by hydrological model; blue boundaries are land side with attenuated oscillations of ground water level:

$$\begin{cases} p = \rho g \cdot (h_{gw}(t) - y) & \text{for } y \leqslant h_{gw}(t), \\ p = 0 & \text{for } y > s(t) \end{cases}, \quad (5)$$

Table 1
LiveDike pressure sensors measurements: relative pressure amplitudes and time delays between the tide and local pressure fluctuations.

Sea water level sensor data						
Sea level drop 258 cm = 253 mbar				Time of local maximum 9.01.2010 5.00		
	Pore pressure sensors data					
	Slice1	Slice2	Slice3	Slice1	Slice2	Slice3
	Relative daily oscillations amplitude (fraction of tidal daily oscillations amplitude)			Time delay between local pressure maximum and sea level maximum, minutes		
E4	0.21	0.11	0.10	18	3	18
E3	0.09	0.10	0.07	24	9	38
G2	0.03	0.08	0.04	49	19	9

Table 2
LiveDike – soil parameters, including calibrated diffusivities.

Van Genuchten parameters			Young's modulus E (Pa)	Poisson's ratio ν	Friction angle φ (°)	Cohesion c (Pa)
α (1/m)	n	l				
8	1.5	0.5	10^{10}	0.3	30	0

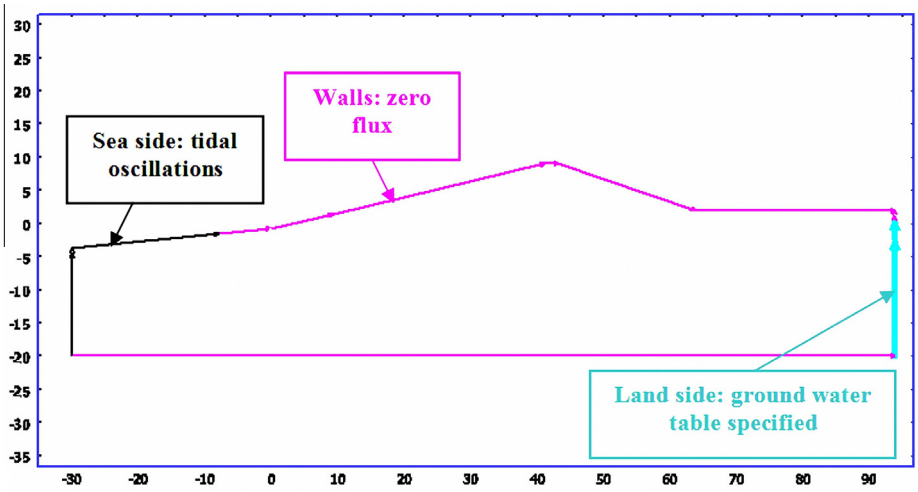

Fig. 7. 2D simulation domain and boundary conditions.

where $h_{gw}(t)$ denotes oscillating ground water level, representing attenuated and altered tidal signal.

In the regime of forced tidal oscillations the initial condition in (1) does not affect the steady solution, due to dissipation of the initial pore pressure distribution within several tidal periods. We have specified a hydrostatic distribution below $y = 0$ m as an initial condition:

$$\begin{cases} p = -\rho g y & \text{if } y \leqslant 0, \\ p = 0 & \text{if } y > 0 \end{cases}.$$

In the saturated zone, where $\theta_e = 1$, $C = 0$, $k_r = 1$, porous flow is modeled by linear and parabolic Laplace equation:

$$\frac{\partial p}{\partial t} + \nabla \cdot \left[-\frac{K_S}{S\mu} \nabla (p + \rho g y) \right] = 0, \tag{6}$$

where $d = \frac{K_S}{S\mu}\,(\mathrm{m}^2/\mathrm{s})$ is soil–water diffusivity, the only soil parameter that influences pore pressure dynamics under the specified load.

The structural sub-model describes stress–strain state of the dike under hydraulic load, gravity and volumetric pore pressure load obtained from flow simulation. Linear elastic – perfect plastic deformations of the soil skeleton are described by the general equations of plastic flow theory (Hill, 1950):

$$\begin{cases} \nabla \cdot \underline{\underline{\sigma}} - \nabla p + \rho_s \underline{g} = 0 \\ \underline{\underline{\sigma}} = \frac{E}{1+\nu} \left[\frac{\nu}{(1-2\nu)} \varepsilon \underline{\underline{I}} + \underline{\underline{\varepsilon}} \right], \quad \text{if } F < 0, \\ \dot{\underline{\underline{\varepsilon}}}_{pl} = -q \frac{\partial F}{\partial \underline{\underline{\sigma}}}, \dot{\underline{\underline{\varepsilon}}} = \dot{\underline{\underline{\varepsilon}}}_{pl} + \frac{1}{3K} I_1 \underline{\underline{I}}, \quad \text{if } F = 0 \end{cases}, \tag{7}$$

where ρ_s is soil density; $\underline{g}$ is gravity vector; $\underline{\underline{\sigma}}$ is effective stress tensor (compressive stresses are negative); E is Young's modulus; ν is Poisson's ratio; $\varepsilon = \varepsilon_{xx} + \varepsilon_{yy} + \varepsilon_{zz}$ is volume deformation (positive for expansion); $\underline{\underline{I}}$ is unit tensor; $\underline{\underline{\varepsilon}} = (\nabla \underline{U} + (\nabla \underline{U}^T)/2$ is deformation tensor; $\underline{U}$ is vector of displacements; $\dot{\underline{\underline{\varepsilon}}}_{pl}$ is plastic deformation rate tensor; q is plastic multiplier; F is plastic yield function; $K = \frac{E}{3(1-2\nu)}$ is bulk modulus; $I_1 = \sigma_{xx} + \sigma_{yy} + \sigma_{zz}$ is the first stress invariant.

Plastic flow has been modeled with a modification of Drucker–Prager plasticity model, optimized for plane strain problems by providing the best approximation of Mohr–Coulomb surface in stress space for 2D cases (Chen and Mizuno, 1990):

$$F = \alpha \cdot I_1 + \sqrt{J_2} - F_{DP},$$

where $J_2 = I_1^2/3 - I_2$ is second deviatoric stress invariant, $I_2 = \sigma_{xx} \cdot \sigma_{yy} + \sigma_{zz} \cdot \sigma_{yy} + \sigma_{xx} \cdot \sigma_{zz} - \sigma_{xy}^2$ is second stress invariant; α and F_{DP} are material constants: $\alpha = tg(\varphi)/\sqrt{9 + 12 \cdot tg^2(\varphi)}$, $F_{DP} = 3c/\sqrt{9 + 12 \cdot tg^2(\varphi)}$; c, φ are cohesion and internal friction angle, respectively.

Boundary conditions for the structural sub-model of the LiveDike are specified as follows:

- A roller condition at the vertical borders: $\underline{n} \cdot \underline{U} = 0; \sigma_{xy} = 0$ (zero normal displacements and zero shear stresses at the boundary).
- The base of the dike is fixed: $\underline{U} = 0$ (zero vector of displacements) at the bottom horizontal border.
- Normal pressure acting below transient sea level at the slopes of the dike:

$$\begin{cases} n \cdot \underline{\underline{\sigma}} = -\rho g \cdot (h(t) - y) & \text{if } y \leqslant h(t), \\ n \cdot \underline{\underline{\sigma}} = 0 & \text{if } y > \text{water level}(t) \end{cases}.$$

Differentiation in (7) is performed with respect to pseudo-time with an initial condition $\underline{\underline{\varepsilon}}_{pl} = 0$.

Eqs. (1) and (7) describe a one-way coupled fluid–structure interaction system. In (1) we did not take into account squeezing/suction of pore water with the volume deformation of the pores (source intensity is zero in (1)). This assumption has been made for the LiveDike as it constructed from sand which usually develops minor pore compaction/expansion.

Table 2 gives a list of soil parameters that have been set for the LiveDike using reference properties of sand.

Water viscosity is calculated as a linear interpolation function of water temperature between the points defined in Table 3. Fig. 8 shows water temperature measurements over a period of 1 year. Due to the variation of water viscosity, the value of soil diffusivity in summer is 1.8 times higher than in winter.

Table 3
Water viscosity values.

Temperature (°C)	Dynamic viscosity (Pa s)
20	1.004×10^{-3}
10	1.307×10^{-3}
0	1.797×10^{-3}

4. Implementation details

In the *Virtual Dike* module, Eqs. (1) and (7) are solved in the finite element package COMSOL 3.5a. A finite element mesh

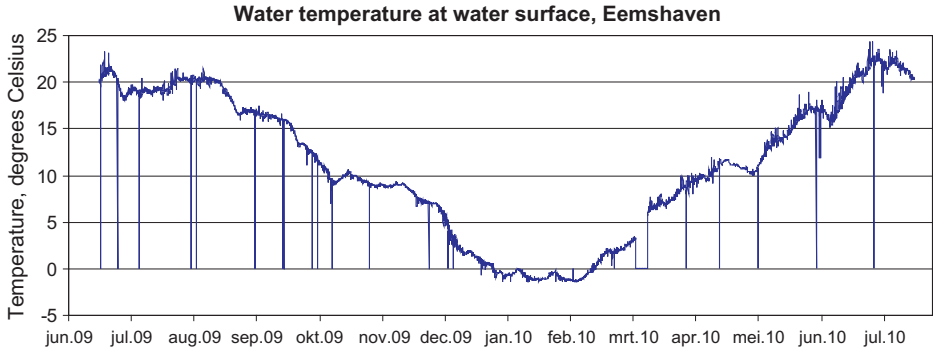

Fig. 8. Sea water temperature measured over a period of 1 year.

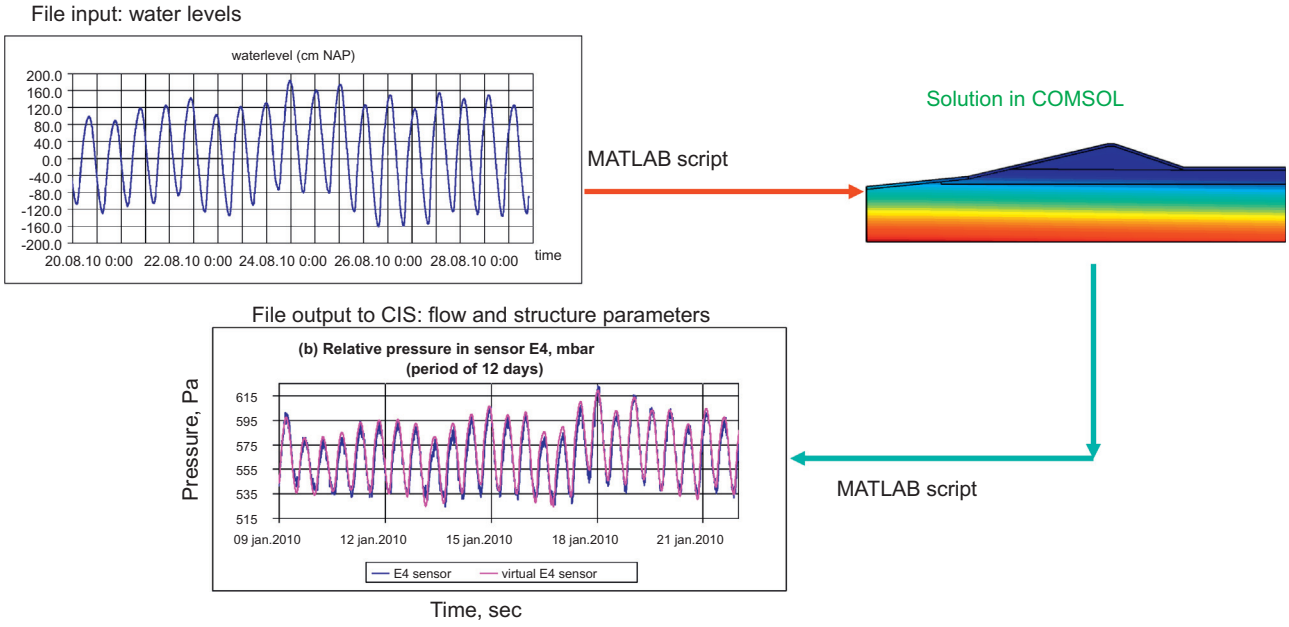

Fig. 9. Virtual Dike simulation workflow.

composed of triangle elements with second order of spatial approximation is used in simulations. Time integration is performed by an implicit backward second order method. The Newton–Raphson iteration scheme is used for solving non-linear algebraic equations at each time integration step. During Newton–Raphson iterations, systems of linear algebraic equations are solved by direct PARDISO solver from the BLAS library.

The *Virtual Dike* module has been integrated into the Common Information Space (CIS) (Balis et al., 2011) on the platform of the national Dutch supercomputing system SARA (http://www.sara.nl/). The module runs in real time, receiving water level sensor signal as input data and producing "virtual sensor" signals (flow and structure parameters).

To start a new simulation, CIS launches a Linux Ubuntu virtual machine with the *Virtual Dike* model and writes sensor input (sea level value) to the specified directory in real-time (updating it every 5 min). The output from the *Virtual Dike* is stored in a specified directory on a hard drive, from where it is accessed by the CIS, compared to sensor measurements and visualized at the user front-end.

Within the *Virtual Dike* module, automatic sensor input is implemented by running MATLAB script, which monitors the input directory for new input files, reads input data, starts COMSOL simulation and stores virtual sensor output (see Fig. 9 for the internal *Virtual Dike* simulation workflow).

5. Sensitivity analysis of pressure amplitude and time delay to the variation of soil diffusivity

Sensitivity analysis has been performed to study the influence of saturated soil–water diffusivity on tidal oscillations of pore pressure in the dike. A 2D homogeneous dike model has been considered. Geometric prototype of the model is the LiveDike's slice. Boundary conditions' zones have been described in Section 3. At the seaside harmonic tidal pressure oscillations are specified; at the landside constant ground water level is specified (zero meters from average sea level). A number of porous flow simulations have been performed, with saturated diffusivities varied in the range of 0.1–1000 m^2/s. Water viscosity was constant: $\mu = 0.001$ Pa s. Distribution of relative pore pressure amplitudes, normalized to tidal amplitude, is presented in Fig. 10a, for a horizontal slice of the dike (at the level $y = -5.5$ m).

For relatively high values of diffusivity ($d = 10$–1000 m^2/s) relative pressure amplitude distribution is linear with a very small non-linear tail close to the sea-side (left) slope. The non-linear part

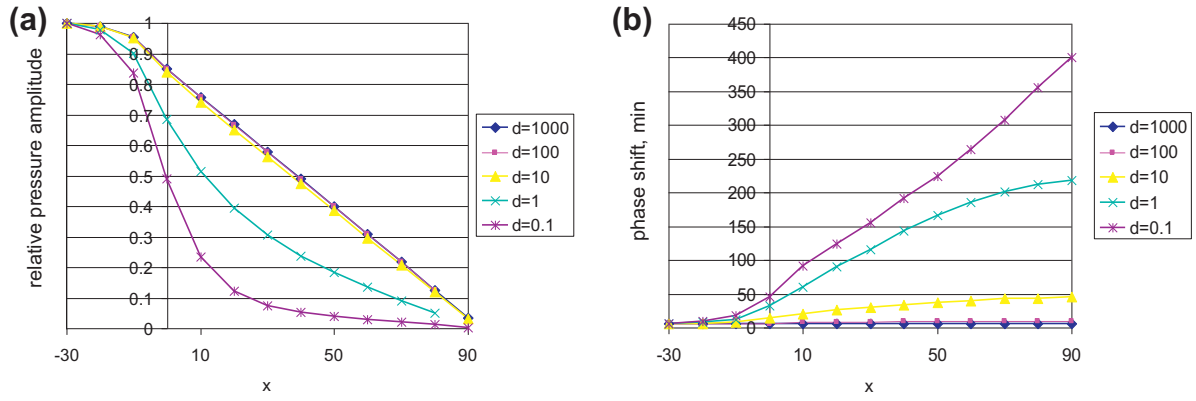

Fig. 10. (a) Relative pressure amplitude distribution along the dike. (b) Time delay distribution along the dike. Data shown in a horizontal slice $y = -5.5$ m (at the level of the E4 sensor, see Fig. 3b).

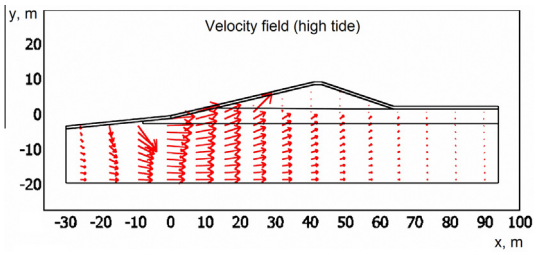

Fig. 11. Arrow plot of velocity field (high tide). The flow is essentially two-dimensional at $x \leqslant 0$ m.

corresponds to the zone where the flow is essentially two-dimensional: at $x \leqslant 0$ m, water penetrates into the domain both through the vertical boundary and through the under-water slope of the dike (see Fig. 11 for arrow plot of flow velocity). At $x \geqslant 0$ m the flow is almost one-dimensional, and relative pressure amplitude distribution qualitatively agrees with the 1D analytical solution presented below (Section 6).

Fig. 10a clearly shows that relative pressure amplitude for loose, permeable media (like gravel and coarse sand) is insensitive to the actual value of diffusivity (lines for $d = 1000$, $d = 100$, and $d = 10$ coincide). This linear distribution is only defined by the amplitude of sea oscillations and by the length of the domain. To the contrary, time delay is sensitive to the value of diffusivity in the whole range (Fig. 10b), therefore time delay can be calibrated by tuning diffusivity value.

For diffusivities $d \leqslant 1$ m^2/s, a significant non-linearity appears in the pressure amplitude distribution: pore pressure amplitude within the dike depends on the diffusivity.

Fig. 12 presents pressure amplitude and time delay as functions of diffusivity, in LiveDike E4 sensor location (50; −5.5). The amplitude and phase delay values of E4 sensor are shown in Fig. 12 with dashed lines.

From Fig. 12 it is clear that matching both the amplitude and phase lag with only one parameter (diffusivity) is impossible: matching the amplitude value requires diffusivity $d \sim 1$ m^2/s, while matching the time delay requires that $d \sim 100$ m^2/s. Formally, besides the diffusivity, one more parameter is necessary to match the data for one sensor. In fact, this contradiction indicates presence of heterogeneity in the LiveDike soil build-up (while the prototype dike in sensitivity analysis is homogeneous). Thus we construct a model of a dike as a set of horizontal stripes, each stripe divided into a number of homogeneous sectors with constant diffusivity. The length of a sector is the second parameter necessary for matching sensor data (Fig. 13). Fig. 13 presents a scheme of construction of a heterogeneous dike model to match sensor data. Sensors E_1, E_2, G_1 are not taken into consideration in the model as they are located above the phreatic surface and they do not produce data on pore pressure. For six values to match (these are pressure amplitude and time delay for three sensors: E_4, E_3, G_2), 6 parameters have been used: lengths of homogeneous zones L_1, L_2 and diffusivities d_1, d_2, d_3, d_4 (see Fig. 13). After calibration a total length of the simulation domain equals to the sum of parameters L_1 and L_2.

6. Analytical analysis of tidal propagation in a one-dimensional homogeneous aquifer

In this section two analytical solutions for the problem of harmonic flow in a one-dimensional saturated homogeneous aquifer are derived and compared to the direct numerical solutions which were discussed in Section 5. A one-dimensional analytical model can be used for modeling tidal propagations through the aquifers with a low gradient of the phreatic line.

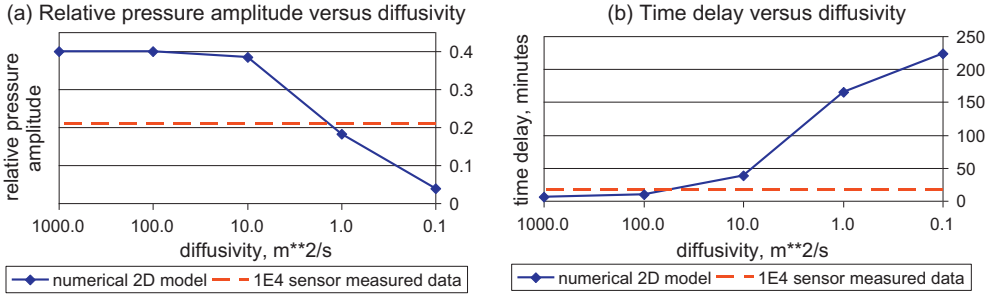

Fig. 12. Influence of soil diffusivity on (a) relative pore pressure amplitude and (b) time delay in 1E4 sensor location (50 m; −5.5 m). Actual values shown with dashed lines.

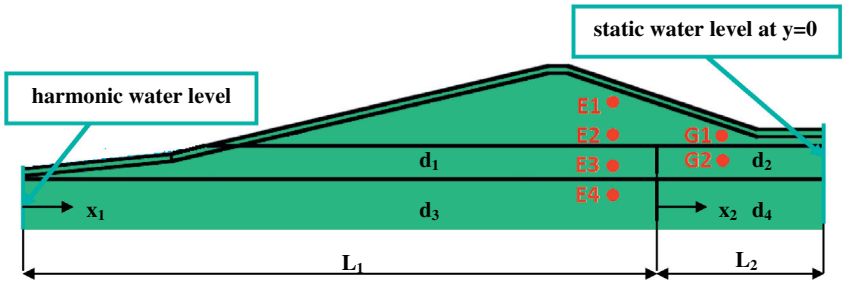

Fig. 13. Construction of a heterogeneous dike model to match sensor data.

The objectives for employing one-dimensional analytical models for dike diffusivity calibration are:

- Obtaining formulas for initial guess values of diffusivity.
- Qualitative study of penetration of tidal waves through the dike.

Flow in a one-dimensional saturated aquifer is described by the equation

$$\frac{\partial p}{\partial t} - d \cdot \frac{\partial^2 p}{\partial x^2} = 0, \tag{8}$$

Harmonic boundary conditions defining two problems are considered:

- A semi-infinite aquifer with sine oscillations of water pressure at the boundary $x = 0$:

$$\begin{aligned} p(x,t)|_{x=0} &= A\sin(\omega t) \\ p(x,t)|_{x\to\infty} &\to 0 \end{aligned}, \tag{9}$$

where A is amplitude of pressure oscillations and ω is angular frequency.

- A finite aquifer with sine pressure oscillations at $x = L$ and constant pressure $p = 0$ at $x = 0$:

$$\begin{aligned} p(x,t)|_{x=L} &= A\sin(\omega t) \\ p(x,t)|_{x=0} &= 0 \end{aligned}. \tag{10}$$

The solution for the semi-infinite aquifer problem (8) with boundary conditions (9) is expressed as follows (Ferris, 1951):

$$p(x,t) = Ae^{-x\sqrt{\frac{\omega}{2d}}} \cdot \sin\left[\omega\left(t - x\sqrt{\frac{1}{2d\omega}}\right)\right]. \tag{11}$$

It represents a wave of pore pressure traveling in compressible soil, with an amplitude p_A (Pa) dissipating exponentially with the distance from the inlet, and a time delay Δt (s) growing linearly with the distance:

$$p_A(x) = Ae^{-x\sqrt{\frac{\omega}{2d}}}, \quad \Delta t = x\sqrt{\frac{1}{2d\omega}}. \tag{12}$$

Applying solution (11) to the model of the dike described in Section 5 (for $-30 \leqslant x \leqslant 90$) we get distributions of relative pressure amplitude $p_A(x)/A$ and time delay Δt (in a logarithmic scale), presented in Fig. 14a and b. Diffusivity d varied in the range between 0.1 and 1000 m^2/s. Tidal frequency $\omega = 2\pi/T$, where $T = 12$ h 25 min.

Fig. 14a gives an estimate for a distance of tidal waves penetration into a homogeneous aquifer. For dense impermeable soils with diffusivity $d \leqslant 0.1$ pressure amplitude dissipates to a level of 4% of tidal amplitude, within the distance of 120 m from the sea. For highly permeable soils with diffusivity $\geqslant 10$ m^2/s, pressure amplitude distribution is linear in the whole domain, and this linear distribution has been confirmed by 2D numerical analysis (Section 5).

According to formula (12), slow seasonal water table fluctuations propagate further into an aquifer than daily fluctuations do, and this was taken into consideration for the LiveDike when specifying land side boundary conditions in the porous flow problem (Section 7).

For the finite aquifer problem (8) with boundary conditions (10), solution representing steady harmonic oscillations and satisfying zero boundary condition $p(x,t)|_{x=0} = 0$ can be expressed as a sum of two complex conjugated independent partial solutions of (8):

$$p = Ce^{i\omega t}\sinh\left(\sqrt{\frac{i\omega}{d}}x\right) + \overline{C}e^{-i\omega t}\sinh\left(\sqrt{-\frac{i\omega}{d}}x\right), \tag{13}$$

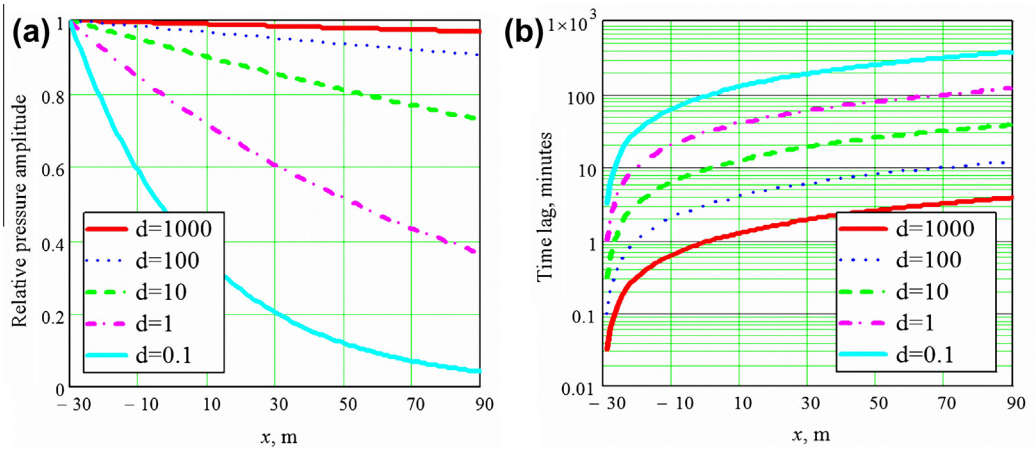

Fig. 14. Analytical solution of 1D problem of tidal oscillations in semi-infinite saturated aquifer. (a) relative pressure amplitude distribution along the domain and (b) time lag, minutes, along the domain – in a logarithmic scale.

where $i = \sqrt{-1}$; $C = \mathrm{Re}(C) + i \cdot \mathrm{Im}(C)$ is a complex constant to be determined from the harmonic boundary condition:

$$p(x,t)|_{x=L} = A\sin(\omega t) \Longleftrightarrow C(\cos(\omega t) + i\cdot\sin(\omega t)) \times \sinh\left(\sqrt{i\frac{\omega}{d}}L\right) + \overline{C}(\cos(\omega t) - i\cdot\sin(\omega t)) \times \sinh\left(\sqrt{-i\frac{\omega}{d}}L\right) = A\sin(\omega t), \quad (14)$$

From (14) follows that:

$$C = \frac{A}{2i\sinh\left(\sqrt{i\frac{\omega}{d}}L\right)}, \quad (15)$$

(13) + (15) ⇒

$$p(x,t)| = 2\mathrm{Re}\left\{\frac{A\cdot\sinh\left(\sqrt{i\frac{\omega}{d}}x\right)}{2i\cdot\sinh\left(\sqrt{i\frac{\omega}{d}}L\right)}(\cos(\omega t) + i\cdot\sin(\omega t))\right\}, \quad (16)$$

Taking into account that

$$\sinh\left(\sqrt{\frac{i\omega}{d}}L\right) = \cos\left(\sqrt{\frac{\omega}{4d}}L\right)\sinh\left(\sqrt{\frac{\omega}{4d}}L\right) + i\cdot\sin\left(\sqrt{\frac{\omega}{4d}}L\right)\cosh\left(\sqrt{\frac{\omega}{4d}}L\right), \quad (17)$$

(16) can then be written as:

$$p(x,d,L,t) = p_A(x)\cdot\sin(\omega(t-\Delta t)),$$

$$p_A(x,d,L) = A\sqrt{\frac{\cosh\left(x\sqrt{\frac{\omega}{d}}\right) - \cos\left(x\sqrt{\frac{\omega}{d}}\right)}{\cosh\left(L\sqrt{\frac{\omega}{d}}\right) - \cos\left(L\sqrt{\frac{\omega}{d}}\right)}}, \quad (18)$$

$$\Delta t(x,d,L) = \begin{cases} \frac{1}{\omega}\cdot arctg\left[\frac{\exp r1}{\exp r2}\right] & if\ \ \exp r2 > 0 \\ \frac{1}{\omega}\left(\pi + arctg\left[\frac{\exp r1}{\exp r2}\right]\right) & otherwise \end{cases},$$

where

$$\exp r1 = -\sinh\left(\sqrt{\tfrac{\omega}{4d}}(x+L)\right)\cdot\sin\left(\sqrt{\tfrac{\omega}{4d}}(x-L)\right) + \sinh\left(\sqrt{\tfrac{\omega}{4d}}(x-L)\right)\cdot\sin\left(\sqrt{\tfrac{\omega}{4d}}(x+L)\right),$$
$$\exp r2 = \cosh\left(\sqrt{\tfrac{\omega}{4d}}(x+L)\right)\cdot\cos\left(\sqrt{\tfrac{\omega}{4d}}(x-L)\right) - \cosh\left(\sqrt{\tfrac{\omega}{4d}}(x-L)\right)\cdot\cos\left(\sqrt{\tfrac{\omega}{4d}}(x+L)\right). \quad (19)$$

Expression (18) describes distributions of relative pore pressure amplitude and of oscillations' time lag along the bounded aquifer (sees Fig. 15 for graphical representation of these distributions).

For dense soils with diffusivity $d \leqslant 1$ m^2/s, the analytical model predicts non-linear profiles of pressure distribution, however the absolute values of pore pressure do not agree with the 2D numerical simulation. For example, for $d = 1$ m^2/s, analytical relative pressure amplitude in point $x = 50$ m $P_A = 0.511$, while in the 2D numerical solution simulated amplitude $P_A = 0.2$.

Possible sources of mismatch between the two models are two-dimensional flow behavior at the sea-side and diffusion of water above the phreatic line, which is considered in the 2D numerical model only.

Calibration of the LiveDike soil parameters based on the sensitivity analysis is described in Section 7.

7. Calibration of diffusivities for the LiveDike

Calibration has been performed for the first slice of the dike. As it was mentioned in Section 5, we have to find the values of six parameters: lengths of homogeneous zones L_1, L_2 and diffusivities d_1, d_2, d_3, d_4 (see Fig. 13). Below we describe the procedure of diffusivity calibration using measured data from three sensors: E3, E4 and G2 in Fig. 13. The algorithm is generic and can be used for any number of sensors in a dike slice.

Initial estimate values of L and d parameters are obtained by superposition of analytical solutions derived from the solution (18) for various periodic boundary conditions:

- In the 1st zone ($d = d_1$, $0 < x_1 < L_1$): $p_1(x_1,t) = p_{11}(x_1,t) + p_{12}(x_1,t)$, where $p_{11}(x_1,t)$ is a solution of (8) with the boundary conditions:

$$p_{11}(x_1,t)|_{x_1=0} = A\sin(\omega t), \quad p_{11}(x_1,t)|_{x_1=L_1} = 0, \quad (20)$$

and $p_{12}(x_1,t)$ is a solution of (8) with the boundary conditions:

$$p_{12}(x_1,t)|_{x_1=0} = 0, \quad p_{12}(x_1,t)|_{x_1=L_1} = A_{interface1}\sin(\omega t + \varphi_{interface1}). \quad (21)$$

Here A is tidal amplitude, ω is tidal frequency, $A_{interface1}$, $\varphi_{interface1}$ are local amplitude and phase delay on the interface of zones #1 and #2 (not known a priory, to be determined from a continuity condition (23).

Table 4
Calibrated values of diffusivities and homogeneous zones' lengths.

(Horizontal diffusivity) (water viscosity) (Pa m^2)				Zone lengths	
$d_1\ \mu$	$d_2\ \mu$	$d_3\ \mu$	$d_4\ \mu$	L_1 (m)	L_2 (m)
0.1×10^{-3}	0.01×10^{-3}	0.9×10^{-3}	0.01×10^{-3}	82	13

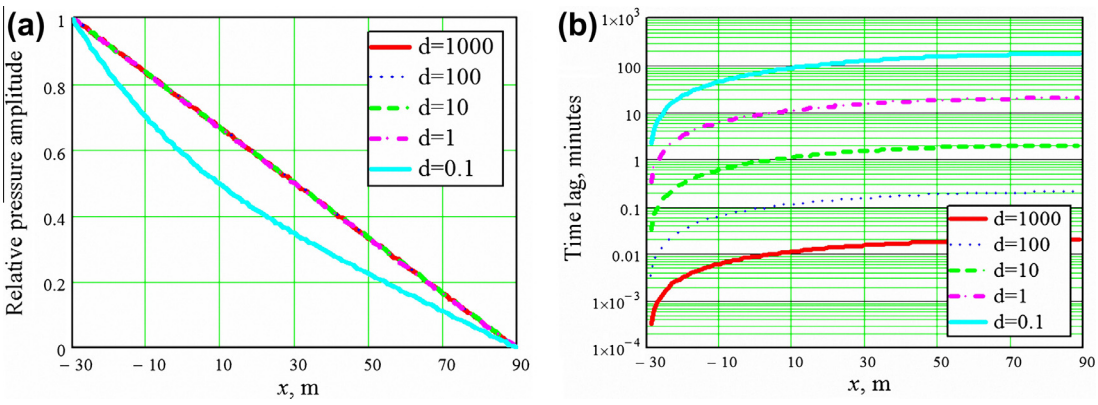

Fig. 15. Analytical solution of 1D problem of tidal oscillations in bounded saturated aquifer. (a) relative pressure amplitude distribution along the domain and (b) time lag, minutes, along the domain – in a logarithmic scale.

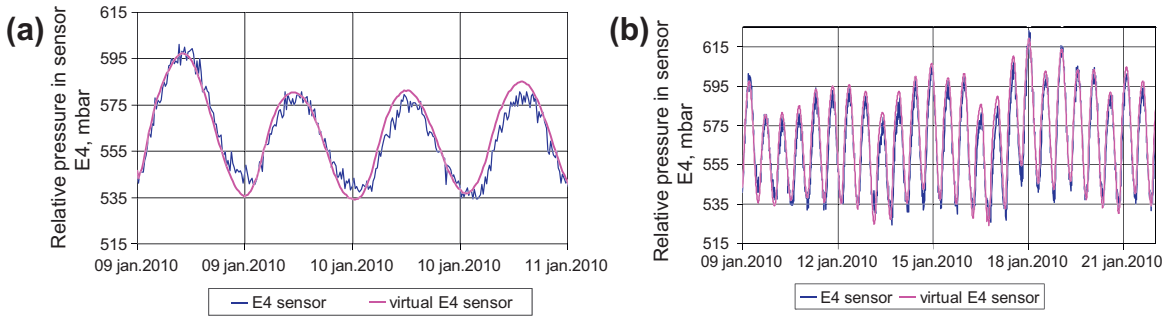

Fig. 16. Relative pore pressure oscillations in sensor 1E4 with calibrated soil properties: (a) Comparison of real sensor data (blue) with simulation results (magenta) on a training dataset. (b) The same, for a longer period of 12 days. (For interpretation of the references to color in this figure legend, the reader is referred to the web version of this article.)

- In the 2nd zone ($d = d_2$, $0 < x_2 < L_2$): $p_2(x_2, t)$ is a solution of (8) with the boundary conditions:

$$p_2(x_2,t)|_{x_2=0} = A_{interface1}\sin(\omega t + \varphi_{inetrface1}),$$
$$p_2(x_2,t)|_{x_2=L_2} = 0.$$

- Continuity condition for the interface between 1st and 2nd zones states that the value of flow velocity does not change at the interface:

$$\frac{\partial}{\partial x_1}p_1(x_1,t)\Big|_{x_1=L_1} = \frac{\partial}{\partial x_2}p_2(x_2,t)\Big|_{x_2=0}. \quad (23)$$

From Eq. (23), we obtain two independent conditions: one for oscillation amplitude $A_{interface1}$ and one for oscillation phase $\varphi_{interface1}$.

- In the 3rd zone: $(d = d_3,\ 0 < x_1 < L_1)$: $p_3(x_1, t) = p_{31}(x_1, t) + p_{32}(x_1, t)$, where $p_{31}(x_1, t)$ is a solution of (8) with the boundary conditions:

$$p_{31}(x_1,t)|_{x_1=0} = A\sin(\omega t), \quad p_{31}(x_1,t)|_{x_1=L_1} = 0, \quad (24)$$

$p_{32}(x_1, t)$ is a solution of (8) with the boundary conditions:

$$p_{32}(x_1,t)|_{x_1=0} = 0, \quad p_{32}(x_1,t)|_{x_1=L_1} = A_{\text{interface2}}\sin(\omega t + \varphi_{\text{interface2}}), \quad (25)$$

where $A_{interface2}$, $\varphi_{interface2}$ are unknown local amplitude and phase delay on the interface of zones #3 and #4.

- In the 4th zone ($d = d_4$, $0 < x_2 < L_2$): $p_4(x_2, t)$ is a solution of (8) with the boundary conditions:

$$p_4(x_2,t)|_{x_2=0} = A_{\text{interface2}}\sin(\omega t + \varphi_{inetrface2}),$$
$$p_4(x_2,t)|_{x_2=L_2} = 0. \quad (26)$$

- Continuity condition for the interface between 3rd and 4th zones is:

$$\frac{\partial}{\partial x_1}p_3(x_1,t)\Big|_{x_1=L_1} = \frac{\partial}{\partial x_2}p_4(x_2,t)\Big|_{x_2=0}. \quad (27)$$

Similar to (23) and (27) gives two scalar conditions: one for oscillation amplitude and one for oscillation phase.

Eqs. (23) and (27) together with six conditions equating amplitudes and time lags in virtual sensors with those in real sensors E3, E4, G2 form a system of 10 scalar equations to determine the initial guess values for the parameters L_1, L_2, d_1, d_2, d_3, d_4, $A_{interface1}$, $\varphi_{interface1}$, $A_{interface2}$, and $\varphi_{interface2}$.

To find more accurate values of d_1, d_2, d_3, d_4 we run numerical simulations as described in Section 4, compare the results with real sensor data and tune the parameters. For a training period of 48 h, the following parameters values have been obtained (Table 4).

Simulation results for a "training" period are shown in Fig. 16a, for the E4 pressure sensor.

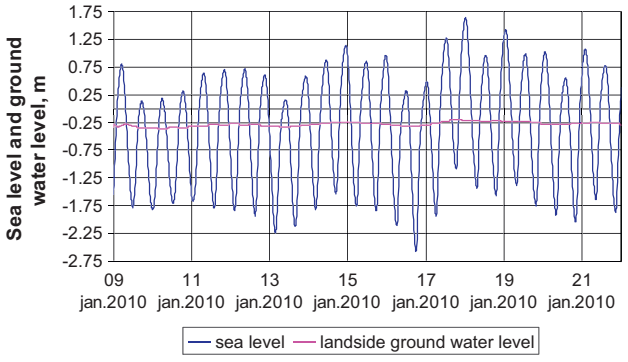

Fig. 17. LiveDike calibration: sea level $h(t)$ and attenuated ground water level $h_{gw}(t)$ at the land side boundary.

For long-term behavior, slow attenuated fluctuations of the ground water level $h_{gw}(t)$ at the land side of the dike should be represented in the boundary condition. Long-term simulations for January 2010 and August 2009 periods have been performed. The attenuated signal $h_{gw}(t)$ has been obtained by averaging the tidal signal $h(t)$ with a 1-day sliding window and multiplying it by a dissipation coefficient q: $h_{gw}(t) = q \cdot h(t)_{averaged}$ (see Fig. 17 for January ground water table plot). The value of q varied depending on the season ($q = 0.15$ for January and $q = 0.25$ for August). Looking at Fig. 17, we can see that the averaged tidal signal represents slow oscillations with the period varying between 2 and 3 days. Variation of the dissipation coefficient q with the season qualitatively agrees with the analytical solution (12) for propagation of slow fluctuations in homogeneous aquifer: according to (12), $q = e^{-x\sqrt{\frac{\pi}{Td}}} \Rightarrow q_{august} = e^{-(L_1+L_2)\sqrt{\frac{\pi}{Td}}} = 0.28$, where homogeneous aquifer diffusivity $d = 0.1$ m^2/s, for slow oscillations with period $T = 48$ h, aquifer length $L_1 + L_2 = 95$ m; $\Rightarrow q_{january} = e^{-(L_1+L_2)\sqrt{\frac{\pi}{Td}}} = 0.18$, for the aquifer with diffusivity $d = 0.1/1.8$ m^2/s (which is summer diffusivity scaled by $\mu_{january}/\mu_{august}$), $T = 48$ h, $L_1 + L_2 = 95$ m.

8. Conclusions

A finite element solver for the analysis of earthen dikes stability has been developed and integrated into the *UrbanFlood* early warning system for early flood protection, where the simulation can be run with the real-time input from water level sensors or with predicted high water levels due to upcoming storm surge or river flood. In the first case, comparison of simulated pore pressures with real data can indicate a change in soil properties or in dike operational conditions (e.g. failure of a drainage pump). In the

second case, simulation can predict the structural stability of the dike and indicate the "weak" spots in the dikes that require attention of dike managers and city authorities.

Mathematical and finite element models of earthen dike behavior under dynamic hydraulic load have been developed. Transient flow through porous media was modeled by Richards' equation with Van Genuchten model for water retention in a partially saturated zone above the phreatic surface.

Sensitivity analysis of porous flow to soil diffusivity showed that:

1. Distribution of pore pressure amplitudes across the dike (in horizontal direction from the sea) is close to linear for highly permeable soils (like gravels and coarse sands) and is significantly non-linear for non-permeable soils, such as clays.
2. Pressure amplitude for coarse media ($d \geqslant 10\ m^2/s$) is insensitive to the value of diffusivity, and is only defined by the boundary conditions.
3. Time delay is always sensitive to the value of diffusivity and can be calibrated by choosing an appropriate saturated diffusivity to match sensor data.

A generic procedure for calibration of diffusivities in a heterogeneous dike has been proposed and successfully tested on the Live-Dike (Groningen). Calibration has been performed on the tidal datasets obtained from real pore pressure sensors. Simulation results with calibrated soil parameters match experimental data, not only on the "training set" but also for a much longer period of time.

The one-dimensional harmonic solution discussed above qualitatively agrees with the 2D numerical solution; the analytical solutions are employed in the numerical model to get initial guess values for diffusivities in the heterogeneous soil build-up.

Our future plans include implementing the program for fully automatic diffusivities calibration, with the algorithm based on the generic calibration procedure described above.

Acknowledgements

This work is supported by the EU FP7 project *UrbanFlood*, Grant No. 248767; by the Leading Scientist Program of the Russian Federation, contract 11.G34.31.0019; and by the BiG Grid project BG-020-10, # 2010/01550/NCF with financial support from The Netherlands Organization for Scientific Research NWO. It is carried out in collaboration with AlertSolutions, Deltares, IJkDijk Association, Rijkswaterstaat, SARA Computing and Networking Services, Waterschap Noorderzijlvest.

References

Balis, B., Kasztelnik, M., Bubak, M., Bartynski, T., Gubala, T., Nowakowski, P., Broekhuijsen, J., 2011. The UrbanFlood common information space for early warning systems. Proced. Comput. Sci. 4, 96–105. http://dx.doi.org/10.1016/j.procs.2011.04.011.

Bathe, K.-J., Khoshgoftaar, M.R., 1979. Finite element free surface seepage analysis without mesh iteration. Int. J. Numer. Anal. Meth. Geomech. 3 (1), 13–22.

Bear, J., 1979. Hydraulics of Groundwater. McGraw-Hill, New York.

Brooks, R.H., Corey, A.T., 1966. Properties of porous media affecting fluid flow. J. Irrig. Drainage Div., ASCE Proc. 72 (IR2), 61–88.

Chen, W.F., Mizuno, E., 1990. Nonlinear Analysis in Soil Mechanics. Elsevier, Amsterdam, Oxford, New York, Tokyo.

Fenton, G.A., Griffiths, D.V., 1997. A mesh deformation algorithm for free surface problems. Int. J. Numer. Anal. Meth. Geomech. 21 (12), 817–824.

Ferris, J.G., 1951. Cyclic fluctuations of water as a basis for determining aquifer transmissibility. IAHS Publ. 33, 148–155.

Gouldby, B., Krzhizhanovskaya, V.V., Simm, J., 2010. Multiscale modeling in real-time flood forecasting systems: From sand grain to dike failure and inundation. Proced. Comput. Sci. 1, 809. http://dx.doi.org/10.1016/j.procs.2010.04.087.

Hill, R., 1950. The Mathematical Theory of Plasticity. Oxford University Press, Oxford.

Krzhizhanovskaya, V.V., Melnikova, N.B., 2012. Modeling earthen dikes: sensitivity analysis and calibration of soil properties based on sensor data. In: Vigo-Aguiar, J. (Ed.), CMMSE 2012: Proceedings of the 12th International Conference on Mathematical Methods in Science and Engineering, vol. IV, Murcia, Spain, 02–05 July, 2012, pp. 1414–1424, ISBN: 978-84-615-5392-1. <http://gsii.usal.es/~CMMSE/images/stories/congreso/4-cmmse-2012.pdf>.

Krzhizhanovskaya, V.V., Shirshov, G.S., Melnikova, N.B., Belleman, R.G., Rusadi, F.I., Broekhuijsen, B.J., Gouldby, B.P., Lhomme, J., 2011. Flood early warning system: design, implementation and computational modules. Proced. Comput. Sci. 4, 106–115. http://dx.doi.org/10.1016/j.procs.2011.04.012.

Meigh, A.C., 1987. Cone Penetration Testing – Methods and Interpretation. Elsevier Science & Technology Books.

Melnikova, N.B., Shirshov, G.S., Krzhizhanovskaya, V.V., 2011a. Virtual dike: multiscale simulation of dike stability. Proced. Comput. Sci. 4, 791–800. http://dx.doi.org/10.1016/j.procs.2011.04.084.

Melnikova, N.B., Krzhizhanovskaya, V.V., Shirshov, G.S., Shabrov, N.N., 2011b. Virtual dike and flood simulator: parallel distributed computing for flood early warning systems. In: Proc. International Conference on Parallel Computational Technologies (PAVT-2011). Publ. Centre of the South Ural State University, Chelyabinsk, pp. 365–373. <http://omega.sp.susu.ac.ru/books/conference/PaVT2011/short/139.pdf>.

Mordvintsev, A., Krzhizhanovskaya, V.V., Lees, M., Sloot, P.M.A., 2012. Simulation of city evacuation coupled to flood dynamics. In: Proceedings of the 6th International Conference on Pedestrian and Evacuation Dynamics, ETH, Zurich, pp. 156–158.

Pengel, B., Krzhizhanovskaya, V.V., Melnikova, N.B., Shirshov, G.S., Koelewijn, A.R., Pyayt, A.L., Mokhov, I.I., 2013. Flood early warning system: sensors and internet. In: Chavoshian, A., Takeuchi, K. (Eds.), IAHS Red Book, No. 357, Floods: From Risk to Opportunity, IAHS Press, pp. 445–453, ISBN 978-1-907161-35-3. <http://iahs.info/redbooks/357.htm>.

Pyayt, A.L., Mokhov, I.I., Lang, B., Krzhizhanovskaya, V.V., Meijer, R.J., 2011a. Machine learning methods for environmental monitoring and flood protection. World Acad. Sci., Eng. Technol. (54), 118–123, <http://waset.org/journals/waset/v54/v54-23.pdf>.

Pyayt, A.L., Mokhov, I.I., Kozionov, A., Kusherbaeva, V., Melnikova, N.B., Krzhizhanovskaya, V.V., Meijer, R.J., 2011b. Artificial intelligence and finite element modeling for monitoring flood defense structures. In: Proc. 2011 IEEE Workshop on Environmental, Energy, and Structural Monitoring Systems, Milan, Italy, pp. 1–7. <http://dx.doi.org/10.1109/EESMS.2011.6067047>.

Slooten, L.J., Carrera, J., Castro, E., Fernandez-Garcia, D., 2010. A sensitivity analysis of tide-induced head fluctuations in coastal aquifers. J. Hydrol. 393, 370–380.

Smith, A.J., Hick, W.P., 2001. Hydrogeology and aquifer tidal propagation in Cockburn Sound, Western Australia. CSIRO Land and Water. Technical Report 6/01.

Spencer, W.A., Hicks, M.A., 2007. A 3D finite element study of slope reliability. Numerical models in geomechanics. In: Proceedings of the Tenth International Symposium on Numerical Models in Geomechanics (NUMOG X), Taylor & Francis Group, London, Rhodes, Greece, 25–27 April, 2007, ISBN 978-0-415-44027-1.

Van Genuchten, M.T., 1980. A closed form equation for predicting the hydraulic conductivity of unsaturated soils. Soil Sci. Soc. Am. J. 44, 892–898.

Verruijt, A., 2001. Soil Mechanics. Delft University of Technology.

Vorogushyn, S., Lindenschmidt, K.-E., Kreibich, H., Apel, H., Merz, B., 2012. Analysis of a detention basin impact on dike failure probabilities and flood risk for a channel-dike-floodplain system along the river Elbe, Germany. J. Hydrol. vols. 436–437, 120–131.

Williams, J.A., Wada, R.N., Wang, R.-Y., 1970. Model studies of tidal effects on ground water hydraulics. Technical Report. Publ. by Water Resources Research Center, University of Hawaii at Manoa. <http://hdl.handle.net/10125/7609>.